Resolving rapidly chirped external fields with Dirac vacuum

C. Gong,[1,2] Z. L. Li,[1] Y. J. Li,[1] Q. Su,[2] and R. Grobe[2]

[1]*State Key Laboratory for GeoMechanics and Deep Underground Engineering, China University of Mining and Technology, Beijing 100083, China*

[2]*Intense Laser Physics Theory Unit and Department of Physics, Illinois State University, Normal, Illinois 61790–4560, USA*

(Received 6 February 2020; accepted 29 April 2020; published 15 June 2020)

We study the dynamical response of the Dirac vacuum state to a very strong time-dependent electric field pulse, whose frequency is chirped in time. The resulting field-induced electron-positron pair-creation process can be used to examine various proposals for time-dependent frequency spectra of the external field. It turns out that the Dirac vacuum can be used as sensitive probe that can respond to the instantaneous values of the frequency at each moment of time by producing electrons with a characteristic energy. This almost instantaneous response feature of the vacuum state permits us to introduce a generalized rate equation. It is based on the concept of a time-dependent decay rate and can provide semianalytical solutions to predict the number of created electron-positron pairs during the interaction with arbitrarily chirped electric field pulses.

DOI: 10.1103/PhysRevA.101.063405

I. INTRODUCTION

To examine the nonlinear response of dynamical systems to an external time-dependent field $E(t)$ from a spectral perspective can be very advantageous, especially if the excitation field is monochromatic and the resulting process is stationary [1]. The traditional spectrum associated with $E(t)$ is usually given here by the Fourier transformation as $S_T(\omega) \equiv |\int_{-\infty}^{\infty} d\tau \exp(-i\omega\tau)E(\tau)|^2$, where the required time integration covers the complete historical record of the field and therefore contains information about the entire pulse. It is obvious that the future behavior of $E(t)$ cannot affect the dynamical response at an earlier time even though it enters the calculation in the Fourier transform. This paradox becomes especially apparent if the signal field is nonmonochromatic and changes its instantaneous frequency during the interaction. A system cannot experience a particular frequency that is provided by the signal in the future.

In order to better describe these temporal changes in the frequency, various ideas have been proposed in the literature to introduce the so-called *time-dependent* spectra. An earlier proposal [2,3] dates back to the 1950s, when Page (and later Lampard) introduced the so-called instantaneous power spectrum. It captures only those spectral features that are associated with the history of the applied signal up to a certain time t, described by $\int_{-\infty}^{t} d\tau \exp(-i\omega\tau)E(\tau)$. Here the upper integration limit is given by t and not by ∞. In order to emphasize the instantaneous character, Page proposed to define an instantaneous power spectrum via the time derivative

$$S_{\rm PL}(\omega;t) \equiv d/dt \left| \int_{-\infty}^{t} d\tau \exp(-i\omega\tau) E(\tau) \right|^2. \quad (1.1)$$

Due to this derivative, $S_{\rm PL}(\omega;t)$ can take negative values, which Page pointed out have to be there in order to partially compensate for unavoidable high frequencies associated with earlier times. This also guarantees that the total energy provided by $E(t)$ up to any time, i.e., $\int_{-\infty}^{t} d\tau\, S_{\rm PL}(\omega;\tau)$, is always positive for all frequencies.

An alternative proposal termed "physical spectrum" was introduced in 1977 by Eberly and Wodkiewicz [4]. They considered in particular the measurement of light pulses and defined their spectrum to be directly related to the counting rate of the photoelectric detector after the light has been transmitted through a Fabry-Perot filter with a characteristic spectral transmission function. This filter introduces in addition to the filter's resonance frequency ω also a finite bandwidth. In the temporal domain, this filter, given by $H(t,\omega,\Gamma)$, restricts the signal and one obtains

$$S_{\rm EW}(\omega;t,\Gamma) \equiv \left| \int_{-\infty}^{\infty} d\tau\, H(\tau - t,\omega,\Gamma)E(\tau) \right|^2. \quad (1.2)$$

Using a moving time window is also inherent to the well-known Gabor transformation [5], where the window function is a Gaussian, i.e.,

$$S_G(\omega;t,w) \equiv \left| \int_{-\infty}^{\infty} d\tau \exp(-i\omega\tau) \times \exp[-(\tau - t)^2/(2w^2)]E(\tau) \right|^2. \quad (1.3)$$

It is invertible and can also provide information on how the phase content of $E(t)$ can change in local sections of the signal as a function of time.

The dynamical significance of these four different definitions of spectra can be examined by their interaction with materials. In the quantum case, the spectrum can sometimes be mapped to the electron's kinetic energy distribution after the photoionization of atoms or molecules. Here the initial state is usually a single or a superposition of discrete energy states, which are then coupled to an energy range of the continuum states.

In this work, we consider a quantum field theoretical system where the initial state is given by a fully occupied

continuum, which can then be coupled by the applied field to a second manifold of continuum states. This situation can be realized by the quantum vacuum state, which is represented by the initially occupied Dirac sea states. We will examine if this vacuum can also act as an agent that can map the time-dependent spectral features of the applied pulse to the energies of the created electron-positron pairs. While neither the Schwinger effect [6] nor the two-photon and multiphoton Breit-Wheeler effect [7] have been observed directly in an experiment [8] yet (without any prior presence of electrons), the possibility to create electron-positron pairs from the vacuum is one of the most striking predictions of quantum electrodynamics. Due to recent progress in the development of high-intensity laser systems, the research area of studying appropriate electromagnetic field configurations to break down the quantum vacuum has triggered some significant interest [9,10].

The main contribution of this work is threefold. First, we will suggest that among the candidates for a time-dependent spectrum, the proposal by Page seems to be in the perturbative regime most relevant to characterize the pair-creation process as it provides a direct relationship to the observed temporal features of the kinetic energy distribution of the created positrons. Second, depending on the external field frequency for quasimonochromatic excitations, we examine different scaling domains of the final particle yield with the field amplitude and construct simple analytical expressions for the power law behavior as well as the transition between the ${E_0}^4$ and ${E_0}^2$ scaling regimes, where E_0 is the amplitude of the field. Finally, we subject the vacuum to a chirped laser pulse [11–15] in both regimes and introduce a fully analytical framework based on the concept of a (time-dependent) vacuum decay rate. It is based on a first-order equation in time that can predict the temporal growth of the total particle yield for chirped force fields.

This article is structured as follows. In Sec. II we compare the various definitions for the time-dependent frequency spectra for a concrete example of chirped pulse of finite duration. We suggest that the Page-Lampard spectrum plays a key role for the pair-creation process in the perturbative regime. In Sec. III we study the perturbative scaling of the final particle yield and nonperturbative deviations for quasimonochromatic fields. In Sec. IV we introduce a rate-based theory to analytically predict the particle yield for chirped external fields. In Sec. V we provide an outlook on open questions and future challenges.

II. TIME-DEPENDENT ENERGY SPECTRA

A. Spectral features

For the numerical studies in this work we have used an oscillatory electric field pulse of duration T, which is characterized by the turn-on and turn-off durations $T_{\rm on}$ and $T_{\rm off}$, the maximum amplitude E_0, an initial frequency ω_0 and a linear chirp parameter b. It is given by

$$E(t) = E_0 f(t) \sin[(\omega_0 + bt/T)t]. \tag{2.1}$$

As shown in Fig. 1(a), the temporal envelope $f(t)$ is given by the three sections: the turn-on region $f(t) = \mathrm{Sin}^2[\pi t/(2T_{\rm on})]$ for $0 \leqslant t \leqslant T_{\rm on}$, the plateau region $f(t) = 1$ for $T_{\rm on} \leqslant t \leqslant T - T_{\rm off}$ and finally the turn-off $f(t) = \mathrm{Cos}^2[\pi(t - T + T_{\rm off})/(2T_{\rm off})]$ for $T - T_{\rm off} \leqslant t \leqslant T$. For a better comparison, in all of our calculations we have kept the specific parameters $T_{\rm on} = T_{\rm off} = 0.01$ a.u. and $T = 0.025$ a.u., such that the plateau region of duration 0.005 a.u. extends from 0.01 a.u. $\leqslant t \leqslant 0.015$ a.u. In view of the relativistic applications of this work, we have used the atomic unit system, where 1 a.u. of time corresponds to 2.42×10^{-17} sec and the electron's mass is 1.a.u., such that the frequency and energy have the same unit as c^2 (with the speed of light $c = 137.036$ a.u.). The rather extended turn-on and turn-off durations relative to the extension of the plateau were necessary in order to keep the energy spectrum (for $b = 0$) sharply localized around $\omega = \omega_0$ with an energy width proportional to 1/T.

The linear-in-time increase of the frequency is described by the chirp parameter b. The time derivative of the phase $(\omega_0 + bt/T)t$ in Eq. (2.1) increases from its initial value ω_0 (at $t = 0$) to its final value $\omega_0 + 2b$. We will see below that it is physically quite meaningful to associate the quantity $\omega_{\rm inst}(t) \equiv \omega_0 + 2(b/T)t$ with an "instantaneous frequency".

The traditional spectrum associated with the chirped $E(t)$ is given $S_T(\omega) \equiv |\int_{-\infty}^{\infty} d\tau \exp(-i\omega\tau)E(\tau)|^2$. It is displayed in the bottom of Fig. 1(b) for $\omega_0 = 2\,c^2$ and $b = 1\,c^2$. We find a wide distribution that covers the range from about $\omega = 2.5\,c^2$ to $\omega = 3.5\,c^2$. Due to the turn-on and off periods, the amplitudes of the early low-frequencies ($\omega = c^2$) and late frequencies ($\omega = 4\,c^2$) are attenuated. For comparison, we have also included the corresponding narrow single-peaked Lorentzian distribution for $b = 0$ (with $\omega_0 = 2.5\,c^2$). As we have outlined in the introduction, this kind of spectrum represents the global features of the entire pulse and therefore does not necessarily uncover appropriately any temporal details during the interaction.

In order to better account for the time-dependent features associated with chirping, we can examine here in more detail two of the three definitions of time-dependent spectra that were mentioned in the introduction. The Gabor and the Eberly-Wodkiewicz time-dependent spectra are similar as they exploit temporal window functions, which introduce a parameter w or Γ. Due to their similarity we focus here only on the Gabor spectrum, which is based on a Gaussian shaped window function of width w as introduced in Eq. (1.3). The numerical value of this width w has to be chosen appropriately. If w is too large, $S_G(\omega;t)$ becomes proportional $S_T(\omega)$ and the spectrum is very wide. If w is chosen too small, the spectrum becomes also very wide as the effective time signal is too narrow to resolve any frequency. In our calculations (where $b = 1\,c^2$), we have chosen an optimal value of $w = [T/(2c^2)]^{1/2}$, which minimizes the spectral width for our particular pulse given by Eq. (2.1) and therefore provides the best possible frequency resolution at any time. This particular estimate for w can be derived, if we assume that the field in Eq. (1.3) is of constant amplitude and simply given by $\sin[(\omega_0 + bt/T)t]$. Here the Gabor spectrum can be determined analytically as being proportional to a Gaussian in frequency, which is centered around $\omega_{\rm inst} = \omega_0 + 2bt/T$ and has a frequency width proportional to $[(a^2 + b^2/T^2)/a]^{1/2}$

$$S_G(\omega;t,w) \sim \exp[-a\,4^{-1}(a^2 + b^2/T^2)^{-1} \times (\omega - \omega_0 - 2bt/T)^2], \tag{2.2}$$

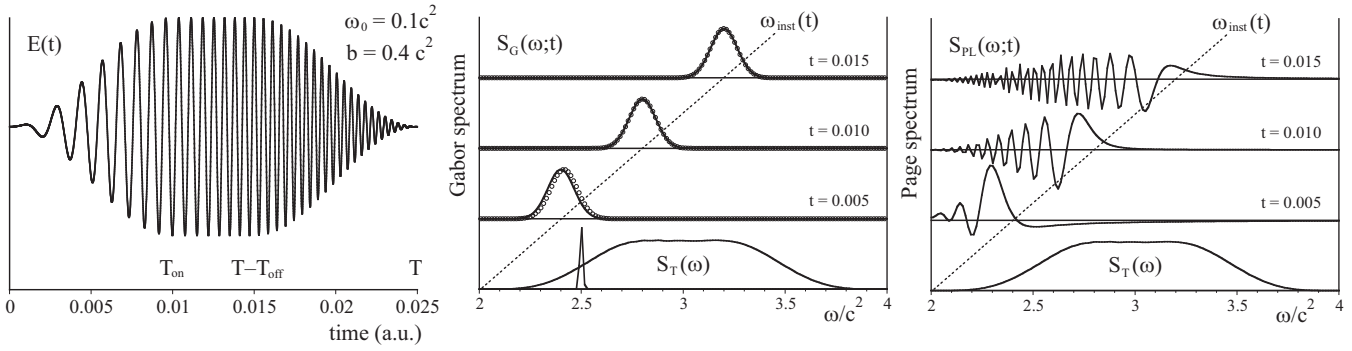

FIG. 1. (a) Sketch of the temporal behavior of the chirped electric field pulse $E(t)$ used in this work (for better visualization of the chirping, it is graphed for $\omega_0 = 0.1\,c^2$ and $b = 0.4\,c^2$). (b) The open circles are the Gabor spectrum $S_G(\omega;t)$ taken at times $t = 0.005$, 0.010 and 0.015 a.u. for $E(t)$ with $\omega_0 = 2c^2$ and $b = c^2$. The continuous lines are the analytical approximations of Eq. (2.2). The bottom graph is the traditional spectrum $S_T(\omega)$ of $E(t)$. For comparison, we also show the spectrum $S_T(\omega)$ for the quasimonochromatic limit $b = 0$ and $\omega_0 = 2.5\,c^2$. (c) The Page-Lampard $S_{\rm PL}(\omega,t)$ spectrum taken at the same times $t = 0.005$, 0.010 and 0.015 a.u. The temporal parameters of $E(t)$ were given by $T_{\rm on} = 0.01$ a.u., $T_{\rm off} = 0.01$ a.u., $T = 0.025$ a.u., $\omega_0 = 2\ c^2$ and $b = c^2$).

where the inverse width parameter is $a \equiv 1/(2w^2)$. One can easily see that the particular choice $a = b$ minimizes the frequency width, which then leads to $w = [T/(2\,c^2)]^{1/2}$, as mentioned above.

In Fig. 1(b) we have displayed the (normalized) Gabor spectra for three different moments in time, $t = 0.005$, 0.01, and 0.015 a.u. They nicely reflect the central frequencies provided by $E(t)$ at the three instants of time. Even though the analytical estimates of Eq. (2.2) did not include any temporal variations of the amplitude, they reflect the true Gabor spectrum very well. For comparison, we have included the predictions of Eq. (2.2) by the continuous lines in Fig. 1(b). To guide the eye, we have also included the location of the instantaneous frequency $\omega_{\rm inst}$ by the dashed line.

In contrast to the Gabor and Eberly-Wodkiewicz spectra, which remove any temporal information outside the window region, the Page-Lampard spectrum considers the entire signal up to a time t. As pointed out in the original work by Page [2,3], if we perform the time derivative in Eq. (1.1), the instantaneous power spectrum $S_{\rm PL}(\omega;t)$ can also be written for computational convenience as

$$S_{\rm PL}(\omega;t) \equiv 2\,E(t)\int_{-\infty}^{t} d\tau \cos[\omega(\tau - t)]E(\tau). \qquad (2.3)$$

In Fig. 1(c), we present the Page-Lampard spectrum for the same chirped electric field at the same three moments in time. We see that it is qualitatively completely different from the other definitions for time-dependent spectra. $S_{\rm PL}(\omega;t)$ is oscillatory and extends over a much larger frequency range, which is roughly given by $\omega_{\rm min} = \omega_0$ to $\omega_{\rm max} = \omega_{\rm inst}(t)$.

A key question is, of course, which of the two time-dependent types of spectra is physically more meaningful to describe the dynamics of pair-creation triggered by a chirped $E(t)$. In order to address this question, we will discuss first in Sec. II B how the pair-creation process is being modeled numerically.

B. Interaction of $E(t)$ on the quantum vacuum

In order to focus on the results of this article, we refer the reader to numerous references [16–19] that detail how computational quantum field theory can be used to solve the time-dependent Dirac equation. These solutions allow us to predict the time-dependent growth of the number density of created electron-positron pairs $N(t)$ from the vacuum and their momentum distributions $N(p,t)$. The underlying theory is briefly sketched in Appendix A. Following Dirac's main idea (which is fully equivalent to a quantum field theoretical description [20]), the vacuum can be represented by a set of initially occupied energy eigenstates of the Dirac Hamiltonian with negative energy [21]. As the applied field is spatially homogeneous, each initial Dirac sea state is coupled to only a unique single state with positive energy of the same canonical momentum. In other words, the vacuum decay process can be mapped onto the dynamics of mutually decoupled two-level systems, each characterized by momentum p.

There is, however, a crucially important difference between the usual two-level systems of atomic, molecular physics, and quantum optics [22–25], which—due to parity conservation—does not reveal any resonances if an even-order multiple of the photon frequency ω_0 matches the energy difference between upper and lower level. In contrast, the particular two-level system derived from the Dirac equation has time-dependent diagonal couplings, which permit even-order resonances as we will discuss in Sec. III.

As derived in Appendix A, the time dependence of the total number per unit length L of created electron-positron pairs is obtained from the sum of all upper-level populations associated with each two-level system, i.e., $N(t) = L^{-1}\Sigma_p |C_{p;u}(t)|^2$. This means that the momentum distribution of the created particles is directly proportional to $|C_{p;u}(t)|^2$ and the energy distribution can be calculated as $\rho(e_p,t) \equiv |dp/de_p||C_{p;u}(t)|^2$, where $dp/de_p = e_p\,c^{-1}({e_p}^2 - c^2)^{-1/2}$ is the corresponding Jacobian to transform from momentum p to energy $e_p = (c^4 + c^2p^2)^{1/2}$.

In the contour plot of Fig. 2 we analyze the energy-time dependence of the temporal change of this energy density, i.e.,

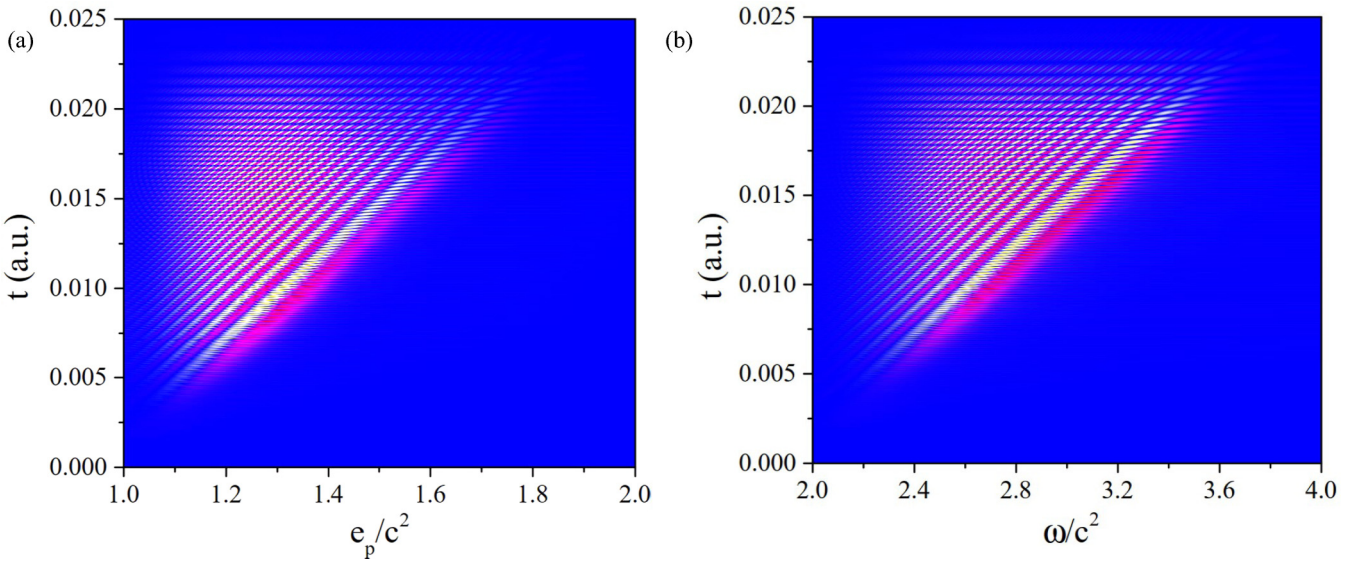

FIG. 2. (a) Contour plot of the temporal derivative of the energy spectrum of the created number of positron $|C_{p;u}(t)|^2$ as a function of the positron energy e_p. (b) The Page-Lampard spectrum $S_{\rm PL}(\omega, t)$ of the external electric force field $E(t)$ (All parameters are the same as in Fig. 1, $T_{\rm on} = 0.01$ a.u., $T_{\rm off} = 0.01$ a.u., $T = 0.025$ a.u., $\omega_0 = 2\,c^2$ and $b = c^2$, $E_0 = 0.005\,c^3$.

$d\rho(e_p, t)/dt$. At any time, the temporal growth of the energy density of the created particles is largest for those energies that match half of the value of the instantaneous frequency of the chirped force field. The Gabor spectra for this pulse [see Fig. 1(b) would (incorrectly) suggest that only those energies should change their density that are close to the instantaneous value of the frequency, $\omega_{\rm inst}(t) = \omega_0 + 2bt/T$. However, the data for $d\rho(e_p, t)/dt$ at time t suggest that $d\rho(e_p, t)/dt$ is quite oscillatory for all energies less than $\omega_{\rm inst}(t)$. In contrast, this feature was predicted by the instantaneous Page-Lampard spectra.

For a direct comparison, we have shown again the spectrum $S_{\rm PL}(\omega; t)$ for the pulse as a contour plot in Fig. 2(b). The quantitative agreement is quite remarkable and clearly suggests that among all definitions of time-dependent frequency spectra, the proposal by Page seems to be physically most meaningful to describe the electron-positron pair-creation process under chirped pulses for these parameter ranges.

The remarkable similarity between the temporal change of the energy distribution of the created positrons and the time-dependent Page-Lampard spectrum can be confirmed analytically. As we pointed out in the appendices, the perturbative solution for the amplitude $C_{p;u}(t)$ can be constructed. If we square its absolute value and take its temporal derivative, we obtain the expression

$$d/dt|C_{p;u}(t)|^2 = 2c^4/e_p^2 A(t) \int_0^t d\tau\, A(\tau) \cos[2\, e_p(t-\tau)]. \tag{2.4}$$

This means that up to the prefactor c^4/e_p^2 in Eq. (2.4), the temporal change of the kinetic energy spectrum of the created positrons takes the identical functional form as the Page-Lampard spectrum of the vector potential $A(t)$, except that we have to replace in the integrand the frequency ω by $2e_p$. This replacement is meaningful as for sufficiently large ω excites positrons with energy $e_p = \omega/2$.

C. Perturbative scaling and nonperturbative deviations for monochromatic fields

Before we examine the more interesting case of the vacuum's response to chirped fields, let us develop first an approximate but fully analytical theory to predict the temporal growth for laser pulses that are not chirped, i.e., $b = 0$. As the underlying physical mechanisms associated with various frequency regions are more different as one might expect, we discuss them separately. To provide a semianalytical simplified description for the temporally induced pair-creation process is in general very difficult. However, if we assume that the electric field amplitude E_0 is not too large and the total pulse duration of the applied field T is not too long, we would expect that the dependence of the final yield $N(T)$ (after the pulse is turned off) might follow a simple power law, $N(T) \sim {E_0}^{2\alpha}$, where the exponent α is a function of the electric field's frequency ω_0.

To examine the numerical value of the exponent for the process, we have computed the final yield $N(T)$ as a function of the applied field's frequency ω_0 for two electric field amplitudes E_0 and $2E_0$. We have repeated the simulation for 100 frequency values ranging from $\omega_0 = 0.6\,c^2$ to a maximum of $\omega_0 = 4c^2$. As these two electric fields differ by a factor of 2, we can then estimate the effective exponent via the logarithm of the ratio

$$\alpha(\omega_0) = \log(4)^{-1} \log[N(T; 2E_0)/N(T; E_0)]. \tag{3.1}$$

In Fig. 3 we have graphed $\alpha(\omega_0)$. In the low-frequency region from about $2c^2/3 < \omega_0 < c^2$ we would expect that the yield is proportional to $\sim E_0^6$, corresponding to $\alpha(\omega_0) = 3$. This integer reflects the minimum number of photons (with energy ω_0), which need to be absorbed to excite the lowest energetic state with $e_p = c^2$ from the lower continuum states with energy $e_p \leqslant -c^2$. The next region (= II) ranging from $c^2 < \omega_0 < 2c^2$ requires the absorption of two photons and therefore the yield should scale quadratic with the intensity,

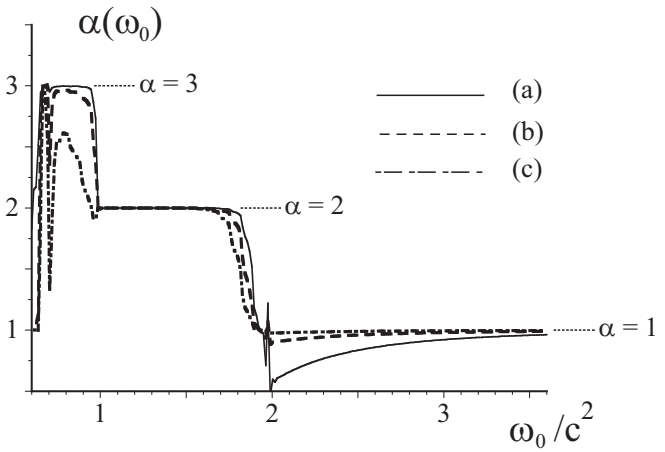

FIG. 3. The effective power law exponent $\alpha(\omega_0)$ [defined in Eq. (3.1)] as a function of the electric field's frequency ω_0. It was obtained numerically from the three ratios of the final particle yields $N(T)$ computed for (a) $E_0 = 0.02\,c^3$ and $0.01\,c^3$, (b) $E_0 = 0.01\,c^3$ and $0.005\,c^3$ and (c) $E_0 = 0.005\,c^3$ and $0.0025\,c^3$. [$T_{\rm on} = 0.01$ a.u., $T_{\rm off} = 0.01$ a.u., $T = 0.025$ a.u.]

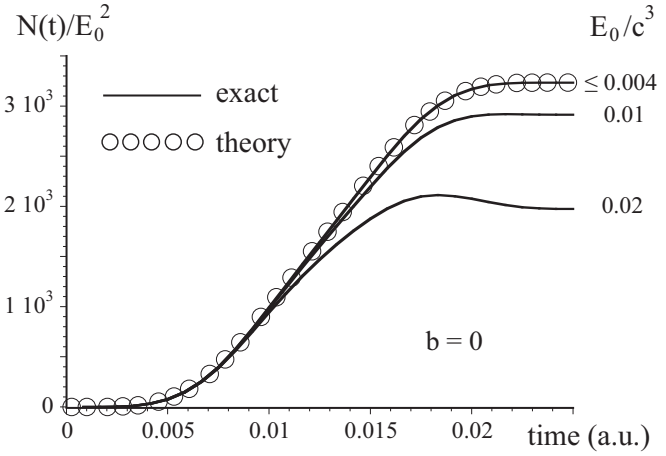

FIG. 4. The temporal growth of the number of created particles $N(t)$ for several electric field amplitudes E_0 in region I for $\omega_0 = 2.2\,c^2$. The open circles are the semianalytical theory based on the rate Eq. (3.2). [$\omega_0 = 2.2\,c^2$, $T_{\rm on} = 0.01$ a.u., $T_{\rm off} = 0.01$ a.u., $T = 0.025$ a.u.]

i.e., $\sim E_0^4$, corresponding to $\alpha(\omega_0) = 2$. Finally, region I for $\omega_0 > 2\,c^2$ has the largest cross section, here the yield is expected to grow linearly with the intensity, $\alpha(\omega_0) = 1$. The computed staircaselike pattern in Fig. 3 confirms the different power law scaling regions.

The observed shifts with regard to the transitions between different scaling regions are an unavoidable consequence of the finite temporal width of the pulse and the resulting nonzero width of the spectral distribution (around ω_0). For example, the spectrum for $\omega_0 = 1.8\,c^2$, contains many frequencies $\omega > 2\,c^2$, that would lead to the $\alpha = 1$ process, that (at least in the perturbative regime) would dominate any other weaker $\alpha = 2$ processes. So even though the center frequency belongs here to the $\alpha = 2$ regime, the final number of particles scale still linearly with the intensity E_0^2.

These threshold shifts illustrate the crucial importance of a relatively long turn-on and -off time required for the electric field to trigger a response other than $\alpha = 1$. To have a concrete example, for $\omega_0 = c^2$, Fig. 3 would reveal a basically constant graph $\alpha(\omega_0) = 1$ for the entire range of all frequencies down to $\omega_0 = 0$, if we had repeated the same simulations using the same total pulse duration ($T = 0.025$ a.u. in this case) but had reduced the turn-on and turn-off durations to zero $T_{\rm on} = T_{\rm off} = 0$. Even though, the pulse $E(t)$ contains about $T/(2\pi/\omega_0) \approx 75$ oscillations, it is far from sufficiently monochromatic in order to lead to a quartic scaling of $N(T)$ with E_0, which we would normally associate with $\omega_0 = c^2$ for truly monochromatic fields with infinite duration.

D. The perturbative region I with $\alpha = 1$

The quadratic scaling of the final number density $N(T)$ as a function of the electric field strength E_0 in region I suggests that the instantaneous change of $N(t)$ for a field pulse $E_0 f(t)$ could be modeled by a rate equation

$$dN(t)/dt = E_0^2 f(t)^2\, \kappa_{\rm I}(\omega_0), \tag{3.2}$$

where the rate constant $\kappa_{\rm I}(\omega_0)$ is exclusively a function of the external field's main frequency ω_0. In order to determine numerically this "cross-section" $\kappa_{\rm I}(\omega_0)$, we have computed the time-dependent growth of $N(t)$. As an example, in Fig. 4 we show $N(t)$ as a function of time for the frequency $\omega_0 = 2.2\,c^2$. We see that during the plateau region ($T_{\rm on} < t < T - T_{\rm off}$), when the amplitude $E_0 f(t)$ is constant ($= E_0$), $N(t)$ grows basically linearly in time in addition to the (nearly invisible) very small oscillations. Using linear regression of $N(t)$ for this regime (sampled over 20 000 temporal points) we can therefore determine the average slope. When we divide this slope by E_0^2, we obtain the desired $\kappa_{\rm I}(\omega_0)$.

In Fig. 5 we have graphed the numerical value of this slope as a function of 300 values for the frequency ω_0. We see that it decreases basically monotonically with increasing ω_0. This means that we would obtain the largest number of

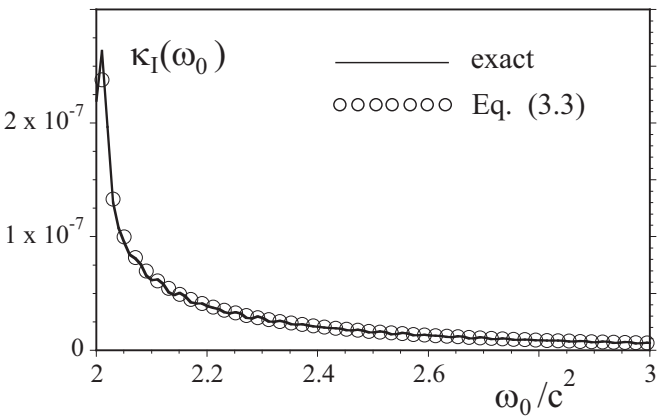

FIG. 5. The scaled cross section $\kappa_{\rm I}(\omega_0)$ for the high-frequency region I as a function of the frequency ω_0. The open circles are the perturbative result according to Eq. (3.3). [$T_{\rm on} = 0.01$ a.u., $T_{\rm off} = 0.01$ a.u., $T = 0.025$ a.u.]

electron-positron pairs if the external field is tuned exactly to the threshold value $\omega_0 = 2\,c^2$.

In Appendix B we apply the usual time-dependent perturbation theory in E_0. As this requires only the solution to a single ordinary differential equation it is possible to obtain a fully analytical estimate for the scaling of $\kappa_{\rm I}(\omega_0)$ with the frequency ω_0.

$$\kappa_{\rm I}(\omega_0) = c^5[(\omega_0/2)^2 - c^4]^{-1/2}\big/\big(2\,\omega_0^3\big). \tag{3.3}$$

This suggests a singularity for the threshold value $\omega_0 = 2\,c^2$. As the derivation of Eq. (3.3) required several approximations, we have to test its validity by comparing it with the exact numerical data obtained from the actual numerically determined slopes of $N(t)$. The open circles in Fig. 5 are the analytical predictions by Eq. (3.3). We find a very good match.

Now that we have an analytical expression for $\kappa_{\rm I}(\omega_0)$, we can use the rate Eq. (3.2) as a much more efficient tool to predict the time-dependent growth for any electric field pulse shape given by $f(t)$. In order to test the accuracy of this approach, we added to the data of Fig. 4 the theoretical prediction based on the solution to Eq. (3.2). We see that for all electric field amplitudes that are less than about $E_0/c^3 = 4 \times 10^{-3}$, the agreement is superb. If the electric field is larger, we begin to enter the nonperturbative region, where the actual (scaled) $N(t)/E_0^2$ is smaller and higher-order perturbative corrections such as level shifts or multiphoton absorptions lead to a lower cross section $\kappa_{\rm I}(\omega_0)$.

E. The perturbative region II where $\alpha = 2$

One could expect that a similar procedure as done for region I could also be applied for the lower-frequency region II, where $c^2 < \omega_0 < 2c^2$. Here we would expect that a similar rate equation given by

$$dN(t)/dt = E_0^4 f(t)^4\,\kappa_{\rm II}(\omega_0) \tag{3.4}$$

could describe the dynamics. While in region I the yield $N(t)$ increases basically monotonically during the field's plateau region after the turn-on, in region II the function $N(t)$ is unfortunately significantly more complicated. We have shown a typical example in Fig. 6.

This function is highly oscillatory with a superimposed envelope that is also nonmonotonic. The specific features of this graph are so complicated as they reveal the simultaneous presence of two different scaling laws. By comparing $N(t)$ for a wide variety of electric field amplitudes, we found that the magnitude of the oscillations scale quadratically in E_0, whereas the final value (after the pulse is turned off) scales quartically, i.e., $N(T) \sim E_0^4$.

This complicated behavior is another manifestation of the inherent fundamental difficulty [26] to cleanly separate between the fully reversible dressing and level shift effects and those irreversible mechanisms, which scale $\sim E_0^4$ and actually do contribute to the final growth of the created particles.

In order to illustrate the transition between the different scaling behaviors, we have graphed the logarithm of the ratio of $N(t)$ for two electric fields ($E_0 = 0.05\,c^3$ and $0.025\,c^3$) that differ by a factor of 2. The transition from $\alpha = 1$ for early times to $\alpha = 2$ for the time after the interaction is obvious from the graph in the inset of Fig. 6.

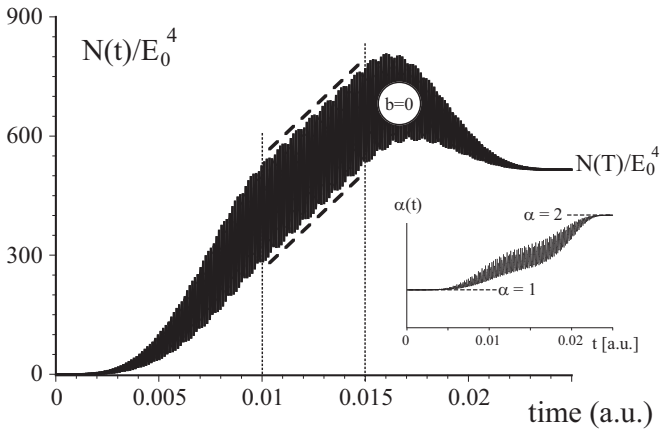

FIG. 6. The temporal growth $N(t)$ of the number of created particles as a function of time in region II for $E_0 = 0.1\,c^3$ and $\omega_0 = 1.3\,c^2$. In the inset we show the scaling of the intensities exponent $\alpha(t) \equiv \log[N(t;2E_0)/N(t;E_0)]/\log(4)$ obtained from the ratio for $E_0 = 0.05\,c^3$ and $E_0 = 0.025\,c^3$. To guide the eye, we have added the dashed lines in the constant amplitude portion $T_{\rm on} < t < T - T_{\rm off}$. [$T_{\rm on} = 0.01$ a.u., $T_{\rm off} = 0.01$ a.u., $T = 0.025$ a.u.]

As the upper and lower envelope of $N(t)$ during the field's plateau region increase linearly in time and have the same slope, we have computed this slope. If we divide it by E_0^4 we can finally compute $\kappa_{\rm II}$ from the data. The result for $\kappa_{\rm II}(\omega_0)$ is shown in Fig. 7 for different frequencies ω_0.

In contrast to the behavior of $\kappa_{\rm I}$ (which was associated with the higher frequency region I), we find that $\kappa_{\rm II}$ does not take its largest coupling at the two-photon threshold value $\omega_0 = c^2$. The maximum is clearly shifted towards higher frequencies.

In order to have also an approximate but analytical estimate of this rate, we have applied in Appendix B the corresponding time-dependent perturbation theory. As we have remarked earlier, the usual two-level system of quantum optics does not reveal any two-photon resonance as observed here. This means that the nature of the perturbation theory applied to the Dirac's two-level dynamics is entirely different. We refer the

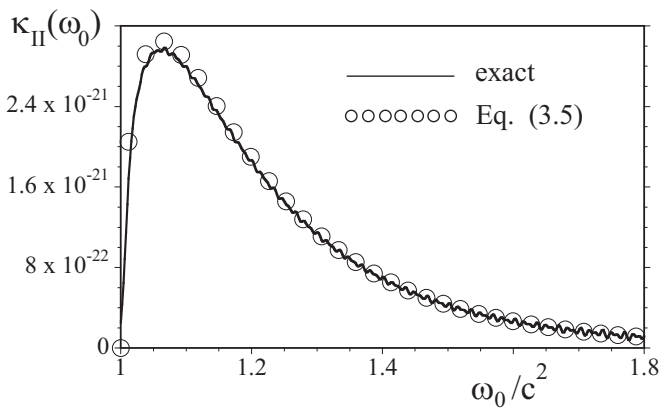

FIG. 7. The scaled cross section $\kappa_{\rm II}(\omega_0)$ for the lower-frequency region II as a function of the frequency ω_0. The open circles are the perturbative result according to Eq. (3.5). [$T_{\rm on} = 0.01$ a.u., $T_{\rm off} = 0.01$ a.u., $T = 0.025$ a.u.]

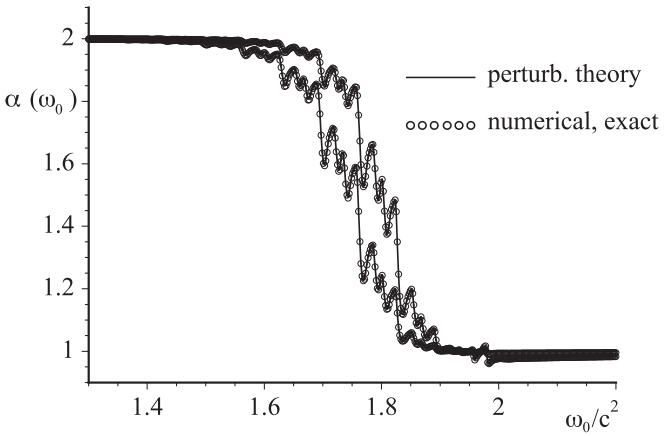

FIG. 8. The effective power law exponent $\alpha(\omega_0)$ [defined in Eq. (3.1)] as a function of the electric field's frequency ω_0 in the transition region for $1.3 < \omega_0/c^2 < 2.2$. It was obtained numerically from the three ratios of the final particle yields $N(T)$ computed for (a) $E_0 = 0.005\,c^3$ and $0.0025\,c^3$ (top curve) and (b) $0.0025\,c^3$ and $0.00125\,c^3$ (bottom curve). The open circles are the analytical prediction based on Eq. (3.6). [$T_{\rm on} = 0.01$ a.u., $T_{\rm off} = 0.01$ a.u., $T = 0.025$ a.u.]

reader here to the interesting discussion in Appendix C and state here only the main result,

$$\kappa_{\rm II}(\omega_0) = c^7(\omega^2 - c^4)^{1/2}/(4\omega^9). \tag{3.5}$$

This expression shows that—in contrast to $\kappa_{\rm I}(\omega_0)$—this cross section does not have any singularity as it decreases to zero for exactly $\omega_0 = 1\,c^2$. As we show in Fig. 7 by the open circles, the agreement with the exact data for all electric fields of amplitude $E_0 < 0.1\,c^3$ is again superb. In order to see any deviations, we have repeated the simulations for large fields that clearly lead to a lower (scaled) particle yield than predicted by lowest-order perturbation theory.

F. The transition region between I and II with effective noninteger power laws

While the frequency regions I and II were characterized by integer exponents α, the most interesting transition domain occurs between these two cases, i.e., for frequencies close to $\omega_0 = 1.8\,c^2$. In order to examine this transition, we have first computed again the final particle yield for two electric field amplitudes $E_0 = 0.005\,c^3$ and $E_0 = 0.0025\,c^3$ for a wide range of frequencies $1.3\,c^2 < \omega_0 < 2.2\,c^2$. Under the (invalid) assumption that also in the transition regime the yield has a simple power law scaling, i.e., $N(T) \sim E_0^{2\alpha}$, we can again compute an effective exponent α via the logarithm of the ratio $\alpha(\omega_0) \equiv \log(4)^{-1}\log[N(T;2E_0)/N(T;E_0)]$ as introduced in Eq. (3.1).

In Fig. 8 we show this exponent α as a function of the frequency ω_0. Quite interestingly, as the frequency increases, the exponent does not decrease from $\alpha = 2$ to $\alpha = 1$ in a monotonic manner as one could have expected. In fact, the overall decrease is superimposed by interesting structures comprised of numerous small local minima and maxima. As these data are computationally difficult to obtain, one could conjecture that these unexpected structures are merely manifestations of numerical inaccuracies. However, we have repeated these simulations for several numerical space-time grids and found the data to be perfectly converged.

Motivated by the accuracy of the perturbative analysis discussed in the appendices, we have generalized these calculations for the transition regime including first-, as well as, second-order terms in E_0.

After a lengthy calculation, we find for the momentum amplitude of the created positrons $C_{p;u}(t)$ the expression given by the two-fold integral

$$C_{p;u}(t) = i\,c^2/(e_p)\exp(-i\,e_p\,t)\int^t d\tau\,A(\tau) \times \exp(2i\,e_p\,\tau)[1 - 2i\,c\,p/e_p\int^\tau A(\tau')d\tau']. \tag{3.6}$$

If at the final time T (after the interaction) we sum the squared absolute values over all final momenta, we obtain again the total number of created positrons, i.e., $N(T) = \Sigma_p|C_{p;u}(T)|^2$. The logarithm of the ratio of $N(T)$ for two electric field amplitudes would then give us a fully analytical (albeit rather complicated) expression for the effective exponents α as a function of ω_0. In Fig. 8 above, the solid lines superimposed on the numerical data (open circles) represent the corresponding prediction based on Eq. (3.6). The perfect agreement is quite remarkable and confirms our numerical finding that the transition between the two $\alpha = 2$ and $\alpha = 1$ perturbative regimes is indeed highly nontrivial.

We should remark that our non-integer exponent α was computed from a specific pair of yield associated with two particular electric field amplitudes E_0. The expression $N(T) \sim E_0^{2\alpha}$ for a non-integer does not mean necessarily a strictly universal scaling for all E_0. In the transition region, $N(T)$ depends mainly on the sum of terms proportional to E_0^2 as well as E_0^4, where the corresponding ω_0-dependent prefactors determine the kind of weighted contribution of each power. In fact, we have repeated the data in Fig. 8 from a different pair of amplitudes E_0 ($= 0.0025\,c^3$ and $0.00125\,c^3$) and observed a very similar transition region. However, the interesting substructures (small maxima and minima) occurred at different values of the frequency ω_0.

The physical causes of these interesting structures are presently unknown but could be examined in a follow up work. As the data were based on the ratios of the final yields, it is possible that they reflect also information about the temporal details of the finite pulses such as the turn-on and off times, about the duration of the plateau region in between, or about the pulse shapes used.

III. PAIR CREATION UNDER RAPIDLY CHIRPED ELECTRIC FIELD PULSES

We have repeated the same simulations as in the prior sections, but this time we have rather rapidly chirped the electric field, i.e., we used $b \neq 0$. Motivated by the remarkable accuracy of the simple rate equation to predict the temporal yield of the particle number density $N(t)$ for a pulsed electric field in region I as well as region II, we can now explore if this approach can be even generalized to account for a chirped electric field. The analysis in terms of the

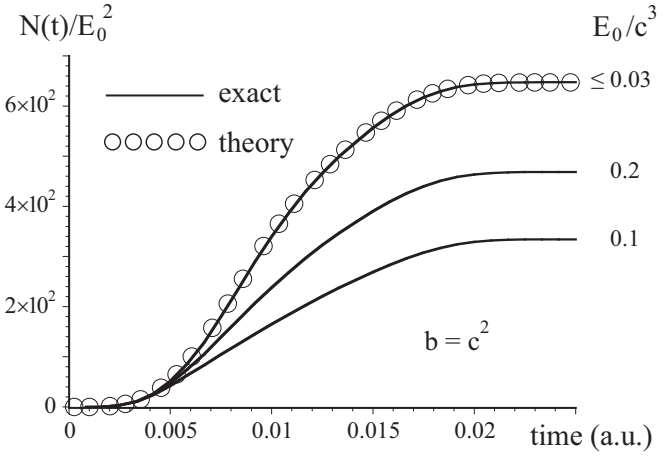

FIG. 9. The temporal growth $N(t)$ of the number of created particles as a function of time in region I for chirping strength $b = c^2$ and $\omega_0 = 2\,c^2$. The open circles are the semianalytical predictions according to the time-dependent rate Eq. (4.1). [$T_{\rm on} = 0.01$ a.u., $T_{\rm off} = 0.01$ a.u., $T = 0.025$ a.u.]

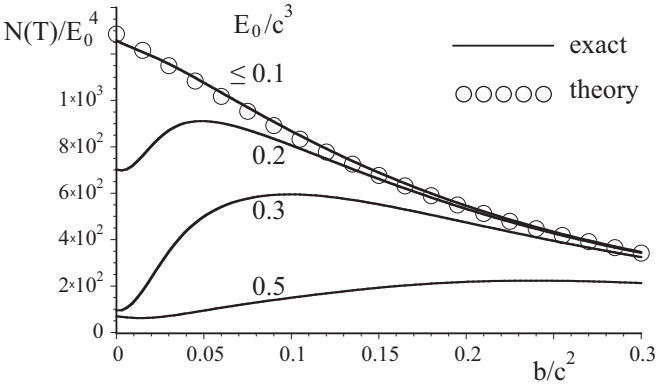

FIG. 10. The final number of created particles $N(T)$ after the interaction as a function of the chirping parameter b for $\omega_0 = 1.1\,c^2$ for four amplitudes E_0. The open circles are the semianalytical predictions according to the time-dependent rate Eq. (4.1). [$T_{\rm on} = 0.01$ a.u., $T_{\rm off} = 0.01$ a.u., $T = 0.025$ a.u.]

time-dependent spectra of $E(t)$ in Sec. II has suggested that the time-dependent instantaneous frequency $\omega_{\rm inst}(t) \equiv \omega_0 + 2bt/T$ is an important characteristic of $E(t)$.

If the vacuum is able to recognize within a very short time-scale this time-changing frequency, one could consider generalizing the rate equation for both region I (with $\alpha = 1$) and II (with $\alpha = 2$) to

$$dN(t)/dt = E_0^{2\alpha} f(t)^{2\alpha} \kappa_\alpha[\omega_{\rm inst}(t)], \tag{4.1}$$

where we have introduced the concept of a time-dependent coupling strength $\kappa_\alpha(t)$.

In Fig. 9 we compare the predictions of the numerical solution $N(t)$ based on Eq. (4.1) for region I, i.e., $\omega_0 = 2\,c^2$ and $b = c^2$ with the exact time evolution. For $E_0 < 0.03\,c^3$ the agreement is superb during the entire interaction. As the frequency (and therefore the coupling strength) changes rapidly even during the field's plateau region, we no longer have a constant-slope region for $N(t)$.

The temporal growth of $N(t)$ for $b = c^2$ covers the large frequency range from $\omega = 2c^2$ to $\omega = 4c^2$. We found that for all amplitudes below the value of $E_0 = 0.03\,c^3$, the solution to the time-dependent rate Eq. (4.1) describes the true growth $N(t)$ very well. We consider the feasibility of this approach to the vacuum decay to be one of the major results of this work. Despite the fact that the instantaneous frequency doubles during the short interaction and the pulse has a nontrivial turn-on and turn-off shape, all details of the entire time evolution of $N(t)$ can be obtained semianalytically with remarkable accuracy, based on the simple analytical form of $\kappa_{\rm I}$ given by Eq. (3.3) and Eq. (4.1).

Quite universally, the agreement is even maintained for region II, where the final yield increases quartically with the amplitude E_0. As we have seen in Sec. III B, due to the simultaneous presence of several scaling laws in region II it is very difficult to provide an unambiguous direct physical meaning to the time dependence of $N(t)$. We therefore have compared the final yield after the interaction $N(T)$ with the solution of the time-dependent rate equation at the final time T in Fig. 10.

We have repeated the simulations for 100 pulses with various degrees of chirping and find for all fields with $E_0 < 0.1\,c^3$ an excellent agreement with the predictions of Eqs. (3.5) and (4.1). Quite interestingly, due to the level shifts in the nonperturbative regime ($E_0 > 0.1\,c^3$), we find that the final yield depends nonmonotonically on the degree of chirping.

IV. SUMMARY AND OPEN QUESTIONS

The traditional linear and nonlinear susceptibilities discussed in classical electromagnetism are proportionality constants relating the amplitude of external field to the resulting polarization of the (usually dielectric) medium. The introduced frequency-dependent functions $\kappa_{\rm I}(\omega_0)$ and $\kappa_{\rm II}(\omega_0)$ serve a similar role as they describe the vacuum's instability towards an external field. Using perturbation theory, it is possible to construct simple but accurate analytical expressions for these nonlinear response functions. It might be very interesting to generalize these expressions for even smaller frequency regimes, with the ultimate goal to find a connection with the zero-frequency limit, where the (intrinsically nonperturbative) Schwinger mechanism dictates the vacuum's decay. To establish this connection is in our opinion a fascinating but not fully understood question. A better understanding of this low-frequency limit is also of fundamental interest for future laser configurations, which are more likely to operate in the lower frequency domain.

This initial work is meant to provide a first proof of fundamental principles and methods rather than mimicking precise laboratory conditions of possible future experiments. A realistic pulse would likely have a central frequency much less than the electron's rest mass. Due to the higher required perturbative order, the resulting analytical expressions for the instantaneous pair-creation rates for lower central frequencies are naturally more complicated. In addition, numerical convergence of time-dependent solutions to quantum field theory is harder to obtain for smaller frequencies of the applied

laser field. For pair-creation processes, an important time scale is about $1/(2\ mc^2)$, associated with the mass gap. Due to the fixed temporal grid spacing, it is numerically challenging to resolve this very rapid time scale, while at the same time having sufficiently long total interaction times, as required by laser fields with small frequencies. Without any further approximations, satisfying both of these two requirements simultaneously would require a horrendous number of temporal grid points, which naturally lead to much longer CPU times and also to numerical convergence that is more difficult to maintain.

By examining the vacuum's response to chirped external fields that scan through a very large frequency range within only a small number of cycles, we have shown that an instantaneous frequency based rate equation approach can provide reliable estimates of the time-dependent growth of the total particle yield. This approach was perturbative and we have shown its limitations for extremely strong fields. Its perturbative validity is likely based on the feature of the quantum vacuum to almost instantly respond to any temporal variation in the spectrum of the field. This would suggest that these truly intrinsic time scales of the vacuum state are extremely short. If the chirping parameter is even much larger, we would expect that the proposed approach might begin to fail, especially when the vacuum's own intrinsic time scales become relevant. To examine these intrinsic time scales, is another worthwhile open challenge, especially, as the vacuum is thought of as being free of any matter. It's presence is usually responsible for the oocurence of dynamical time scales.

While the analysis presented here was focused on positively chirped fields, one may wonder if the conclusions hold also for those fields where the instantaneous frequency decreases as a function of time. For a finite pulse, a negative chirp can be related to the corresponding temporally reversed field with positive chirp. A recent article [27] examined the effect of time-reversed external force fields and suggested that the final electron-positron yield after the interaction is identical for positive and negative chirp if the external field is spatially homogeneous. This resembles the situation considered in the present work. Quite interestingly, if the external force field has also a nontrivial spatial dependence, then the final yield for positive and negative chirp can be different.

Finally, we should mention that we have examined here only the electric response properties of the fermionic Dirac vacuum, modeled by a fully occupied Dirac sea. The true vacuum state of quantum electrodynamics, i.e., the lowest energetic eigenstate of the Hamiltonian describing the fully coupled interaction of electrons, positrons and photons, might possibly reveal additional response features to external excitations. We are certainly just at the early stages of our understanding.

ACKNOWLEDGMENTS

C.G. would like to thank ILP for the hospitality during his visit to Illinois State University and acknowledges the China Scholarship Council program. This work has been supported by the National Science Foundation (NSF) and Research Corporation.

APPENDIX A

In one spatial dimension and the temporal gauge, the Dirac Hamiltonian is given by

$$H = c\,\sigma_1[P - qA(t)/c] + c^2\,\sigma_3, \tag{A1}$$

where P is the momentum operator and we assume the coupling to a positron with charge $q = 1$. The two 2×2 Pauli matrices are denoted by σ_1 and σ_3 and $A(t) = -c\int^t d\tau E(\tau)$ is the vector potential. As the external field $E(t)$ is assumed to be spatially homogeneous in this work, the total canonical momentum is conserved and each initial Dirac sea state is coupled to only a single state in the upper energy continuum state with the same momentum p. In other words, the vacuum decay can be represented by an infinite set of mutually independent two-level systems with energies $-[c^4 + c^2p^2]^{1/2}$ and $e(p) = [c^4 + c^2p^2]^{1/2}$. The lower (labeled d) and upper (labeled u) energy eigenstates $|p;d\rangle$ and $|p;u\rangle$ of H for $A(t) = 0$ take the spatial representation by the two-component spinors, $\langle x|p;u\rangle = N\{[e_p + c^2]^{1/2}, [e_p - c^2]^{1/2}p/|p|\}\exp[i\,p\,x]$ and $\langle x|p;d\rangle = N\{-[e_p - c^2]^{1/2}p/|p|,\ [e_p + c^2]^{1/2}\}\exp[i\,p\,x]$, where N is the corresponding normalization factor. Using the functional form of the two energy eigenstates, the four coupling matrix elements take the form $\langle p;u|\sigma_1|p;u\rangle = c\,p/e_p \equiv a_p$, $\langle p;d|\sigma_1|p;d\rangle = -a_p$ and $\langle p;d|\sigma_1|p;u\rangle = \langle p;u|\sigma_1|p;d\rangle = c^2/e_p \equiv b_p$. The corresponding time-dependent amplitudes in each two-level state $|\Psi_p(t)\rangle = C_{p;d}(t)|p;d\rangle + C_{p;u}(t)|p;u\rangle$ have to fulfill [28]

$$i\,d\,C_{p;u}(t)/dt = [e_p - A(t)a_p]C_{p;u}(t) - A(t)b_p\,C_{p;d}(t), \tag{A2a}$$

$$i\,d\,C_{p;d}(t)/dt = -A(t)b_p\,C_{p;u}(t) - [e_p - A(t)a_p]C_{p;d}(t). \tag{A2b}$$

As we will need it for below, let us perform a unitary transformation to another basis set [28], that is based on the instantaneous lower (D) and upper (U) energy eigenstates $|p;D_t\rangle$ and $|p;U_t\rangle$. These are defined based on the full Dirac Hamiltonian, $H(t)|p;U_t\rangle = e_p(t)|p;U_t\rangle$ and $H(t)|p;D_t\rangle = -e_p(t)|p;D_t\rangle$, where the instantaneous energy eigenvalue takes the form $e_p(t) \equiv [[e_p - A(t)a_p]^2 + [A(t)b_p]^2]^{1/2}$. For a fixed momentum p, the state $|\Psi_p(t)\rangle = C_{p;d}(t)|p;d\rangle + C_{p;u}(t)|p;u\rangle$ can be equally expressed based on the superposition $|\Psi_p(t)\rangle = C_{p;D}(t)|p;D_t\rangle + C_{p;U}(t)|p;U_t\rangle$. The corresponding expansion coefficients $C_{p;D}$ and $C_{p;U}$ are given by the solution to

$$i\,d\,C_{p;U}(t)/dt = \alpha_p(t)\,C_{p;U}(t) + \beta_p(t)C_{p;D}(t), \tag{A3a}$$

$$i\,d\,C_{p;D}(t)/dt = \beta_p^*(t)\,C_{p;U}(t) - \alpha_p(t)C_{p;D}(t), \tag{A3b}$$

where the two matrix elements are given by

$$\alpha_p(t) = [[e_p - A(t)a_p]^2 + [A(t)b_p]^2]^{1/2}, \tag{A4a}$$

$$\beta_p(t) = i\,dA/dt\,c^2/[2\alpha_p(t)^2]. \tag{A4b}$$

In order to avoid an infinite number of created electron-positron pairs, we constrain the length of our interaction region to L, noting that the actual number of created pairs $N(t)$ created by a spatially constant electric field $E(t)$

naturally has to increase linearly proportional to L. This number is computed here by the sum over all of upper state populations, which diverges with increasing L. We therefore introduce the number density, $N(t)$, defined as $N(t)/L$.

In the free basis, this corresponds to $N_{\rm free}(t) = L^{-1}\Sigma_p|C_{p;u}(t)|^2$ and with regard to the instantaneous energy basis, it is given by $N(t) = L^{-1}\Sigma_p|C_{p;U}(t)|^2$. While, in principle, $N_{\rm free}(t)$ and $N(t)$ match only after the pulse $E(t)$ is turned off [28], in the perturbative limit they are similar. We note that the traditional quantum Vlasov equation [29–33] is equivalent to the projection on the instantaneous energy states.

APPENDIX B

In this Appendix we derive the perturbative form of the cross section $\kappa_{\rm I}$ for the high-frequency region. As the differences between Eqs. (A2) and (A3) show up only in higher orders of E_0, both equations lead to the same cross section. For a given momentum p, we assume that in lowest order, Eq. (A2a) simplifies to $i\,dC_{p;d}(t)/dt = -e_pC_{p;d}(t)$. The corresponding solution $C_{p;d}(t) = \exp(i\,e_p\,t)$ is then inserted into the rhs of Eq. (A2a). If we neglect the time-dependent on-diagonal term, the equation can be integrated leading to

$$C_{p;u}(t) = i\,b_p\int^t d\tau\,\exp[-i\,e_p(t-\tau)]\,A(\tau)\exp(i\,e_p\tau). \tag{B1}$$

If we assume a monochromatic field $A(\tau) = c\,E_0/\omega_0[\exp(i\,\omega_0\,t) + \exp(-i\,\omega_0\,t)]/2$, and neglect the term with a too rapidly oscillating phase, we obtain

$$C_{p;u}(t) = i\,b_p\exp(-i\,e_p\,t)c\,E_0/\omega_0\int^t d\tau\,\exp(i\,2e_p\,\tau)\times\exp(-i\,\omega_0\,t)/2, \tag{B2}$$

which can be integrated to

$$C_{p;u}(t) = -b_p\exp(-i\,e_p\,t)\,c\,E_0/(2\omega_0)\times\{\exp[-i\,(\omega_0-2e_p)t]-1\}/(\omega_0-2e_p). \tag{B3}$$

Therefore, the population in the upper level for each two-level system is given by

$$|C_{p;u}(t)|^2 = c^6\,E_0^2\big/\big(4\omega_0^2\big)\,e_p^{-2}\sin^2[(e_p-\omega_0/2)t]/(e_p-\omega_0/2)^2, \tag{B4}$$

where we have also used $b_p = c^2/e_p$. In order to obtain the total population, we have to sum over all individual populations associated with all positive and negative momenta $N(t) = L^{-1}\Sigma_p|C_{p;u}(t)|^2$ where $p_n = n(2\pi/L)$. If we convert the summation to a continuous integral, we obtain

$$N(t) = 1/(2\pi)\,c^6\,E_0^2\big/\big(4\omega_0^2\big)\int dp\,e_p^{-2}\sin^2[(e_p-\omega_0/2)t]/(e_p-w_0/2)^2. \tag{B5}$$

As the next step, we approximate the energy denominator e_p^{-2} by the resonant value $(\omega_0/2)^2$, which allows us to factor this (now p independent) term out of the integral. Due to the inherent symmetry between positive and negative momentum states, we can restrict the summation to positive values. If we use the integral $\int dx\,\mathrm{Sin}^2[xt]/x^2 = \pi t$, we obtain the expression

$$\mathrm{N}(t) = 1/(2\pi)\,E_0^2c^5[(\omega_0/2)^2 - c^4]^{-1/2}\big/\big(2\omega_0^3\big)\pi t. \tag{B6}$$

As a result we obtain for the scaled variable $\kappa_{\rm I}(\omega_0) \equiv E_0^{-2}dN/dt$ the final expression

$$\kappa_{\rm I}(\omega_0) = c^5[(\omega_0/2)^2 - c^4]^{-1/2}\big/\big(2\,\omega_0^3\big).$$

APPENDIX C

The derivation for the rate in region I of Appendix B is similar to the one often employed in quantum optics or atomic physics, see the Fermi Golden rule. The derivation of $\kappa_{\rm II}$, however, provides some interesting physical insight. It is well-known from quantum optics that (due to parity conservation) the traditional two-level system of atomic physics [22–25,34] does not permit any resonance if the energy difference $2e_p$ of the two levels is equal to an *even* multiple of the laser's frequency ω_0. As we have argued above, the two-level system derived from the Dirac equation is conceptually different due to the additional time-dependent on-diagonal coupling elements. In order to better distinguish mathematically between the different dynamical roles of the (same) field $A(t) = A_0\cos(\omega_0 t)$ associated with the diagonal and the off-diagonal couplings, we have temporarily renamed the *on*-diagonal coupling field $A_{\rm on}(t) = A_{\rm on}\cos(\omega_0 t)$. If we introduce the two probability amplitudes $D_{p;d}$ and $D_{p;u}$ defined as

$$D_{p;u}(t) \equiv \exp\left(i\int^t d\tau[e_p - A_{\rm on}(\tau)a_p]\right)C_{p;u}(t), \tag{C1a}$$

$$D_{p;d}(t) \equiv \exp\left(-i\int^t d\tau[e_p - A_{\rm on}(\tau)a_p]\right)C_{p;d}(t), \tag{C1b}$$

then the equations of motion for the variables read

$$i\,d\,D_{p;u}(t)/dt = -b_p\exp\left(2i\int^t d\tau[e_p - A_{\rm on}(\tau)\,a_p]\right)\times A(t)\,D_{p;d}(t), \tag{C2a}$$

$$i\,d\,D_{p;d}(t)/dt = -b_p\exp\left(-2i\int^t d\tau[e_p - A_{\rm on}(t)a_p]\right)\times A(t)D_{p;u}(t). \tag{C2b}$$

This means that the time dependence of the effective force field that couples the variables $D_{p;u}(t)$ and $D_{p;d}(t)$ is no longer solely proportional to $A(t)$, but to the more complicated form $\exp(2i\int^t d\tau[e_p - A_{\rm on}(\tau)a_p])A(t)$, which contains odd as well as *even* order harmonics if the field $A(t)$ is monochromatic. This immediately explains why the Dirac-like two-level system is sensitive to the *even*-order resonances. If we perform the integral in the exponent $\exp(2i\int^t d\tau[e_p - A_{\rm on}(\tau)a_p]) = \exp(2ie_p\,t - 2i(a_pA_{\rm on}/\omega_0)\sin(\omega_0 t))$, then we can apply the Jacobi-Anger expansion for exponentiated trigonometric functions in terms of the n-th Bessel functions of the first

kind, given by $\exp(i\,x\sin t) = \Sigma_n J_n(x)\exp(i\,n\,t)$. As a result, we obtain

$$i\,d\,D_{p;u}(t)/dt = -b_p \exp(2ie_p\,t)\Sigma_n J_n(-2a_p A_{\rm on}/\omega_0)\exp(i\,n\,\omega_0\,t)A(t)D_{p;d}(t), \tag{C3a}$$

$$i\,d\,D_{p;d}(t)/dt = -b_p \exp(-2ie_p\,t)\Sigma_n J_n(2a_p A_{\rm on}/\omega_0)\exp(i\,n\,\omega_0\,t)A(t)\,D_{p;u}(t). \tag{C3b}$$

As we are only interested in the lowest-order perturbative effect due to $A_{\rm on}$, we can expand the Bessel function up to first order as $J_0(x) = 1$, $J_1(x) = x/2$ and $J_{-1}(x) = -x/2$. We obtain

$$\Sigma_n J_n(-2a_p A_{\rm on}/\omega_0)\exp(i\,n\,\omega_0\,t) = 1 - a_p A_{\rm on}/\omega_0 \exp(i\,\omega_0\,t) + a_p A_{\rm on}/\omega_0 \exp(-i\,\omega_0\,t), \tag{C4a}$$

$$\Sigma_n J_n(2a_p A_{\rm on}/\omega_0)\exp(i\,n\,\omega_0\,t) = 1 + a_p A_{\rm on}/\omega_0 \exp(i\,\omega_0\,t) - a_p A_{\rm on}/\omega_0 \exp(-i\,\omega_0\,t). \tag{C4b}$$

We then use $A(t) = A_0[\exp(i\omega_0 t) + \exp(-i\omega_0 t)]/2$ and retain among the eight terms only those ones with the smallest phase factor, which for our frequency range is $\pm(2e_p - 2\omega_0)t$. We, therefore, obtain

$$i\,d\,D_{p;u}(t)/dt = -b_p\,a_p\,A_{\rm on}/\omega_0\,A_0 \exp[i\,2(e_p - \omega_0)t]/2D_{p;d}(t), \tag{C5a}$$

$$i\,d\,D_{p;d}(t)/dt = -b_p\,a_p\,A_{\rm on}/\omega_0\,A_0 \exp[-i\,2(e_p - \omega_0)t]/2D_{p;u}(t). \tag{C5b}$$

Similarly as in Appendix B, in perturbation theory, we can assume $D_{p;d}(t) = 1$ such that we can integrate the first equation from $t = 0$ to t and obtain

$$D_{p;u}(t) = b_p a_p A_{\rm on}/\omega_0 A_0\{\exp[i\,2(e_p - \omega_0)t] - 1\}/[4(e_p - \omega_0)], \tag{C6}$$

such that we obtain for the upper population

$$|D_{p;u}(t)|^2 = |C_{p;u}(t)|^2 = b_p^2\,a_p^2\,A_{\rm on}^2/\omega_0^2\,A_0^2\,\{\sin^2[(e_p - \omega_0)t]/[4(e_p - \omega_0)^2]. \tag{C7}$$

We would like to stress again that here the two-photon-like resonance is proportional to $A_{\rm on}^2\,A_0^2$ and therefore completely absent for the traditional two-level system (for which $A_{\rm on}$ is zero). If we replace $b_p = c^2/e_p$, $a_p = c\,p/e_p$, $A_{\rm on} = A_0 = cE_0/\omega_0$, then this simplifies to $|C_{p;u}(t)|^2 = c^{10}p^2\,E_0^4\,{e_p}^{-4}\,\omega_0^{-6}\,{\rm Sin}^2[(e_p - \omega_0)t)/[4(e_p - \omega_0)^2]$. Finally, if we sum over all final populations (as we did in Appendix B) we obtain

$$N(t) = (1/\pi)c^7\left(\omega_0^2 - c^4\right)^{1/2}/\left(4\omega_0^9\right)E_0^4\,\pi t. \tag{C8}$$

As a result we obtain for the scaled variable $\kappa_{\rm II}(\omega_0) \equiv E_0^{-4}dN/dt$ the final desired expression

$$\kappa_{\rm II}(\omega_0) = c^7\left(\omega_0^2 - c^4\right)^{1/2}/\left(4\omega_0^9\right).$$

[1] L. Mandel and E. Wolf, *Optical Coherence and Quantum Optics* (Cambridge University Press, Cambridge, 1995).
[2] C. H. Page, J. Appl. Phys. **23**, 103 (1952).
[3] D. G. Lampard, J. Appl. Phys. **25**, 803 (1954).
[4] J. H. Eberly and K. Wódkiewicz, J. Opt. Soc. A **67**, 1252 (1977).
[5] D. Gabor, J. Inst. of Elect. Eng. Part III, Radio and Communication, **93**, 429 (1946).
[6] J. S. Schwinger, Phys. Rev. **82**, 664 (1951).
[7] G. Breit and J. A. Wheeler, Phys. Rev. **46**, 1087 (1934).
[8] For recent advances in high power laser systems, see, for example, the web sites of the following labs: ELI (Paris), diocles (Lincoln), xfel (Hamburg), sparc (Darmstadt), Vulcan, HiPER and Astra Gemini (Oxfordshire), polaris (Jena) or Shenguang III (Mianyang), LCLS (Stanford), TPL (Austin) or numerous references in https://eli-laser.eu/.
[9] For a comprehensive review, see, e.g., A. Di Piazza, C. Müller, K. Z. Hatsagortsyan, and C. H. Keitel, Rev. Mod. Phys. **84**, 1177 (2012).
[10] For a recent review, see, B. S. Xie, Z. L. Li, and S. Tang, Matter Radiat. Extremes **2**, 225 (2017).
[11] C. K. Dumlu, Phys. Rev. D **82**, 045007 (2010).
[12] Z. L. Li, H. B. Sang, and B. S. Xie, Chin. Phys. Lett. **30**, 071201 (2013).
[13] H. B. Sang, M. Jiang, and B. S. Xie, Chin. Phys. Lett, **30**, 111201 (2013).
[14] M. Jiang, B. S. Xie, H. B. Sang and Z. L. Li, Chin. Phys. B **22**, 100307 (2013); A. Nurriman, B. S. Xie, Z. L. Li and D. Sayipjamal, Commun. Theor. Phys. **59**, 331 (2013); A. Nurriman, Z. L. Li, and B. S. Xie, Chin. Phys. B **26**, 020301 (2017).
[15] C. Gong, A. Penwell, Z. L. Li, Y. J. Li, Q. Su, and R. Grobe, J. Opt. Soc. Am. B **37**, 1098 (2020).
[16] J. W. Braun, Q. Su, and R. Grobe, Phys. Rev. A **59**, 604 (1999).
[17] U. W. Rathe, P. Sanders, and P. L. Knight, Parallel Comput. **25**, 525 (1999).
[18] C. H. Keitel, Cont. Phys. **42**, 353 (2001).
[19] G. R. Mocken and C. H. Keitel, J. Comp. Phys. **199**, 558 (2004).
[20] T. Cheng, Q. Su, and R. Grobe, Cont. Phys. **51**, 315 (2010).
[21] P. A. M. Dirac and P. A. M. Dirac, Proc. Roy. Soc. Lond. A **117**, 610 (1928).

[22] L. Allen and J. H. Eberly, *Optical Resonance and Two-Level Atoms* (Wiley, New York, 1975).
[23] P. Milonni and J. H. Eberly, *Lasers* (Wiley, New York, 1988).
[24] C. C. Gerry and P. L. Knight, *Introductory Quantum Optics* (Cambridge University Press, Cambridge, 2005).
[25] R. W. Boyd, *Nonlinear Optics* (Academic, New York, 2008).
[26] P. Krekora, Q. Su, and R. Grobe, Phys. Rev. A **73**, 022114 (2006).
[27] See a summary of Ref. [15] by F. Miatto, Spotlight on Optics (OSA, March 2020), https://www.osapublishing.org/spotlight.
[28] J. Unger, S. Dong, R. Flores, Q. Su, and R. Grobe, Laser Phys. **29**, 065302 (2019).
[29] S. Schmidt, D. Blaschke, G. Röpke, S. A. Smolyansky, A. V. Prozorkevich, and V. D. Toneev, Int. J. Mod. Phys. E **7**, 709 (1998).
[30] Y. Kluger, E. Mottola, and J. M. Eisenberg, Phys. Rev. D **58**, 125015 (1998).
[31] J. C. R. Bloch, V. A. Mizerny, A. V. Prozorkevich, C. D. Roberts, S. M. Schmidt, S. A. Smolyansky, and D. V. Vinnik, Phys. Rev. D **60**, 116011 (1999).
[32] R. Alkofer, M. B. Hecht, C. D. Roberts, S. M. Schmidt, and D. V. Vinnik, Phys. Rev. Lett. **87**, 193902 (2001).
[33] C. Kohlfürst, M. Mitter, G. von Winckel, F. Hebenstreit, and R. Alkofer, Phys. Rev. D **88**, 045028 (2013).
[34] *Handbook of Atomic, Molecular, and Optical Physics*, edited by G. W. F. Drake (Springer, New York, 2005).